*Emirates Journal for Engineering Research, 18 (2), 53-61 (2013)*

*(Regular Paper)*

# DEPENDENCE OF BUOYANCY-DRIVEN FLOW INSIDE AN OBLIQUE POROUS CAVITY ON ITS ORIENTATION

**Iman Zahmatkesh**

*Department of Mechanical Engineering, Mashhad Branch, Islamic Azad University, Mashhad, Iran*
*E-mail address: zahmatkesh5310@mshdiau.ac.ir*

*(Received February 2013 and Accepted June 2013)*

اهتمام هذه الورقة يتركز على توضيح كيفية تأثير اتجاه ميل تجويف مسامي مائل على تطور حركي لتدفق الطفو فيه. و لقد تم وضع جدارين متقابلين لتجويف في درجات حرارة ثابتة ولكن عند قيم مختلفة في حين تم عزل الجدارين الآخرين. ولقد تم حل معادلات حفظ الكتلة، والقوة الدافعة، والطاقة عدديا بالاعتماد على العمليات الحسابية المستندة على عنصر تحكم الحجم. وتم مناقشة تكون الاطراب (الانتروبي) تحت تأثير نقل الحرارة الغير مرتجعة و تحت تأثير احتكاك السوائل الغير مرتجع.

وتم التحقق من صحة نموذج الحل العددي بالمقارنة بأعمال منشورة سابقا. وبعد ذلك، تم عرض و مقارنة نتائج المحاكاة العددية لزوايا اتجاه الميل من π/4، 3π/4، 5π/4، و 7π/4. وتبين أن من بين الأمثلة المعروضة، أن أفضل حالة لانتقال الحرارة و لتكون الاطراب (الانتروبي) تتحقق من خلال اتجاهات ميل يكون فيها الجدار الساخنة في الجزء العلوي والجدار البارد في الجزء السفلي.

In the present paper attention is focused to clarify how orientation of an oblique porous cavity may affect the establishment of buoyancy-driven flow therein. Two opposite walls of the cavity are kept at constant but different temperatures while the other two are maintained adiabatic. The mass, momentum, and energy conservation equations are solved numerically adopting a control-volume based computational procedure. The generation of entropy is also discussed taking into account both heat transfer irreversibility and fluid friction irreversibility.

The developed numerical model is validated against previously published works. Thereafter, simulation results are presented for the inclination angles of $\pi/4$, $3\pi/4$, $5\pi/4$, and $7\pi/4$ and the corresponding results are compared. It is demonstrated that, among current cases, the optimum case with respect to heat transfer as well as entropy generation is achieved through the orientations with the hot wall in the top and the cold wall in the bottom.

## 1. INTRODUCTION

Buoyancy-driven flows inside cavities filled with a fluid-saturated porous medium appear in diverse practical situations including cooling of radioactive waste containers, grain storage, terrestrial heat flow through aquifer, and heat exchange in granular insulating materials. Consequently, it is not surprising to see considerable interest in the analysis of these flow problems in the past (e.g., Baytas and Pop [1], Saeid and Pop [2], Misirlioglu et al. [3], and Zahmatkesh [4,5]).

A porous cavity can be oblique or vertical depending on its orientation with respect to gravity. Thereby, some previous attention has been paid to buoyancy-driven flows inside oblique porous cavities. One of the first contributions has been made by Moya et al. [6] who analyzed the consequences of inclination angle on the induced flow and thermal fields inside porous cavities. Free convection in oblique porous cavities with partially cooled walls has been investigated by Oztop [7]. He found that inclination angle is the dominant parameter on heat transfer and fluid flow as well as aspect ratio. The effect of inclination angle has also been examined during numerical simulations of Dawood and Ismaeel [8]. Baytas [9] has studied free convection and entropy generation inside oblique porous cavities. He clarified how inclination angle may affect the distributions of streamlines, isothermal lines, and iso-entropy generation lines. Moreover, he presented the variations of local Nusselt number and global entropy generation rate with the inclination angle. More recently, control of free convection and entropy generation in oblique porous cavities by placing of a partition has been discussed by Heidary et al. [10].

In all of the aforesaid studies, free convection was the sole heat transfer mode that was taken into account. Nevertheless, investigations of Zahmatkesh [11] and Badruddin et al. [12] have demonstrated that, thermal radiation may possess profound consequences on the establishment of the flow and thermal fields inside porous cavities. It makes temperature distribution nearly uniform in vertical sections inside the cavity and causes the streamlines to be nearly parallel with the vertical walls. It may also lead to nearly uniform adiabatic wall temperatures. This indicates that, the inclusion of thermal radiation is crucial when one studies buoyancy-driven flows inside oblique porous cavities.

In the present paper attention is focused to extend previous investigations on oblique porous cavities by incorporating thermal radiation in the heat transfer processes therein. The aim of this study is to find that, among the inclination angles of π/4, 3π/4, 5π/4, and 7π/4, which orientation leads to an optimum case with respect to heat transfer as well as entropy generation. The present cases are geometrically similar and their sole difference is attributed to the selection of the walls to be heated/cooled. To the author's knowledge, the current orientations have not been previously compared from the standpoints of the First Law and the Second Law of thermodynamics.

The present paper is organized as follows. Mathematical formulation of the problem is described in detail in Section 2. The employed solution procedure is outlined in Section 3. Grid independence test and numerical validation are presented in Sections 4 and 5. Simulation results are demonstrated in Section 6. Finally, Section 7 summarizes major findings of the current study.

## 2. MATHEMATICAL FORMULATION

Buoyancy-driven flow inside an oblique cavity filled with a fluid-saturated porous medium is analyzed in this study. A schematics of the porous cavity is depicted in Figure 1. Here, one of the walls is maintained at the temperature of $T_H$ which is warmer than its opposite wall with the temperature of $T_C$. The other two walls are, however, assumed to be adiabatic.

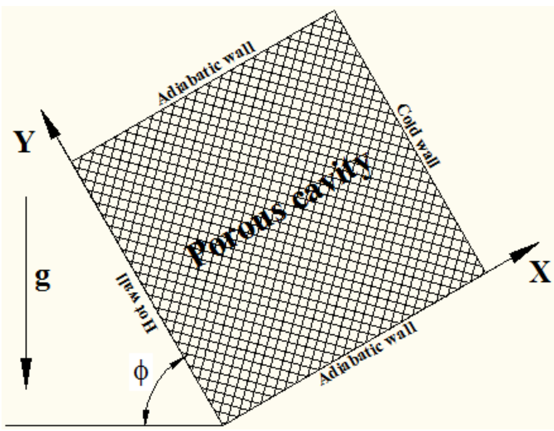


Figure 1. A schematics of the oblique porous cavity.

During the current analysis, Darcy's model with the Oberbeck-Boussinesq approximation is utilized for flow prediction while the Rosseland diffusion approximation [13] is adopted to describe radiation heat transfer. Moreover, radiative heat flux in the y-direction is considered negligible in comparison with that in the x-direction. As a consequence, the conservation equations for the problem at hand take the form of

$$\frac{\partial u}{\partial x}+\frac{\partial v}{\partial y}=0\,, \tag{1}$$

$$u=-\frac{K}{\mu}\frac{\partial p}{\partial x}+\frac{Kg\beta}{\upsilon}\left(T-T_C\right)\cos\phi\,, \tag{2}$$

$$v=-\frac{K}{\mu}\frac{\partial p}{\partial y}+\frac{Kg\beta}{\upsilon}\left(T-T_C\right)\sin\phi\,, \tag{3}$$

$$u\frac{\partial T}{\partial x}+v\frac{\partial T}{\partial y}=\alpha\left(\frac{\partial^2 T}{\partial x^2}+\frac{\partial^2 T}{\partial y^2}\right)-\frac{1}{\rho c_p}\frac{\partial q_r}{\partial x}\,, \tag{4}$$

Eliminating pressure terms from Eqs. (2)-(3) by applying cross-differentiation yields

$$\frac{\partial u}{\partial y}-\frac{\partial v}{\partial x}=\frac{Kg\beta}{\upsilon}\left(\frac{\partial T}{\partial y}\cos\phi-\frac{\partial T}{\partial x}\sin\phi\right). \tag{5}$$

Meanwhile, in the view of Rosseland diffusion approximation, the energy equation becomes [11]

$$u\frac{\partial T}{\partial x}+v\frac{\partial T}{\partial y}=\alpha\left(\frac{\partial^2 T}{\partial x^2}+\frac{\partial^2 T}{\partial y^2}\right)+\frac{16\sigma}{3\rho a c_p}T_C^3\frac{\partial^2 T}{\partial x^2}\,. \tag{6}$$

The corresponding boundary conditions are

$x=0$ and $0<y<L$:

$$u=0\,,\; v=0\,,\text{ and } T=T_H\,. \tag{7a}$$

$x=L$ and $0<y<L$:

$$u=0\,,\; v=0\,,\text{ and } T=T_C\,. \tag{7b}$$

$0<x<L$ and $y=0$:

$$u=0\,,\; v=0\,,\text{ and } \partial T/\partial y=0\,. \tag{7c}$$

$0<x<L$ and $y=L$:

$$u=0\,,\; v=0\,,\text{ and } \partial T/\partial y=0\,. \tag{7d}$$

Introducing stream function (i.e., $\psi$ ) as

$$u=\frac{\partial\psi}{\partial y}\text{ and } v=-\frac{\partial\psi}{\partial x}\,, \tag{8}$$

by which the continuity equation is automatically satisfied, and defining dimensionless parameters in the form of

$$X=\frac{x}{L}\,,\; Y=\frac{y}{L}\,,\; \Psi=\frac{\psi}{\alpha}\,,\; \Theta=\frac{T-T_C}{T_H-T_C}\,,\quad R_d=\frac{4\sigma T_C^3}{ak}\,,\; Ra=\frac{g\beta\Delta TKL}{\nu\alpha}\,, \tag{9}$$

Eqs. (5) and (6) reduce to

$$\frac{\partial^2 \Psi}{\partial X^2} + \frac{\partial^2 \Psi}{\partial Y^2} = Ra\left(\frac{\partial \Theta}{\partial Y} cos\,\phi - \frac{\partial \Theta}{\partial X} sin\,\phi\right), \tag{10}$$

$$\frac{\partial \Psi}{\partial Y}\frac{\partial \Theta}{\partial X} - \frac{\partial \Psi}{\partial X}\frac{\partial \Theta}{\partial Y} = \left(1+\frac{4R_d}{3}\right)\frac{\partial^2 \Theta}{\partial X^2} + \frac{\partial^2 \Theta}{\partial Y^2}. \tag{11}$$

Moreover, the corresponding boundary conditions become

$X = 0$ and $0 < Y < 1$:

$$\Psi = 0 \text{ and } \Theta = 1. \tag{12a}$$

$X = 1$ and $0 < Y < 1$:

$$\Psi = 0 \text{ and } \Theta = 0. \tag{12b}$$

$0 < X < 1$ and $Y = 0$:

$$\Psi = 0 \text{ and } \partial\Theta / \partial Y = 0. \tag{12c}$$

$0 < X < 1$ and $Y = 1$:

$$\Psi = 0 \text{ and } \partial\Theta / \partial Y = 0. \tag{12d}$$

## 3. ENTROPY GENERATION

Following a similar non-dimensionalization procedure, dimensionless rate of entropy generation takes the form of [10]

$$N(X,Y) = \left[\left(\frac{\partial \Theta}{\partial X}\right)^2 + \left(\frac{\partial \Theta}{\partial Y}\right)^2\right] + \frac{Ec\,Pr}{\tau}\left[\left(\frac{\partial \Psi}{\partial X}\right)^2 + \left(\frac{\partial \Psi}{\partial Y}\right)^2\right], \tag{13}$$

with $Ec$ being the Eckert number, $Pr$ being the Prandtl number, and $\tau$ being the dimensionless temperature difference (i.e., $\Delta T/T_C$). Here, the first term on the right-hand side is due to the transfer of heat and is referred to as Heat Transfer Irreversibility (*HTI*) while the second term represents the contribution of Fluid Friction Irreversibility (*FFI*).

As the distribution of entropy generation rate inside the cavity is obtained, it is integrated over the whole domain that yields the global entropy generation rate as

$$N_{global} = \iint_{\forall} N\, d\forall = \int_0^1\int_0^1 N(X,Y)\, dXdY. \tag{14}$$

## 4. SOLUTION PROCEDURE

The dimensionless coupled partial differential equations are solved simultaneously along with the corresponding boundary conditions. For this purpose, a control-volume based computational procedure [14] is adopted. The governing equations are converted into a system of algebraic equations through integration over each control volume. The algebraic equations are thereafter solved by a line-by-line iterative method. The method sweeps the domain of integration along the x and y axes and uses the Tri-Diagonal Matrix Algorithm (TDMA) to solve the system of equations. The employed convergence criterion is the maximum residuals of all variables which must be less than $10^{-5}$. During the current entropy generation computations, the following parameters are maintained constant.

$Ec\,Pr = 0.01$, $\Delta T = 100$ K, and $T_C = 300$ K.

As the conservation equations are solved, the local and the average Nusselt numbers at the non-adiabatic walls are obtained from the following expressions.

$$Nu = -\left[(1+\frac{4R_d}{3})\frac{\partial \Theta}{\partial X}\right]_{X=0,1}, \tag{15}$$

$$\overline{Nu} = \int_0^1 Nu\; dY. \tag{16}$$

## 5. GRID STUDY

To obtain a grid suitable for this study, a grid independence test is performed. Accordingly, simulation results in terms of average Nusselt number at the non-adiabatic walls are listed in Table 1, that corresponds to Ra=100 and $\phi$=π/2. Inspection of the presented results indicates that a $200\times200$ grid provides acceptable results here. Further investigations also verify the suitability of such a grid under other inclination angles.

Table 1. Grid independence test.

| Grid size | $300\times300$ | $200\times200$ | $100\times100$ | $50\times50$ |
|---|---|---|---|---|
| $\overline{Nu}$ | 3.077 | 3.068 | 3.026 | 2.950 |

## 6. NUMERICAL VALIDATION

To establish the accuracy of the present numerical simulation, results of the developed model in terms of average Nusselt number at the non-adiabatic walls and temperature at the adiabatic walls are compared with those of previously published works in Table 2 and Figure 2, respectively. Here, the Darcy-modified Rayleigh number is 100 and the inclination angle is π/2. The contribution of thermal radiation is also disregarded to be similar with previous investigations. Notice that the results of the present model bear a strong resemblance to the previously published works. Moreover, contour plots of stream function and temperature are almost the same as those reported in open literature. They are not, however, presented here for the sake of brevity. This provides confidence to the developed mathematical model as well as the employed solution procedure for further studies. Consequently, in the forthcoming section, they will be utilized to analyze buoyancy-driven flow inside an oblique porous cavity with different orientations.

Table 2. Comparison of the average Nusselt number with previously published works.

| Author | $\overline{\mathbf{Nu}}$ |
|---|---|
| Baytas and Pop [1] | 3.160 |
| Saeid and Pop [2] | 3.002 |
| Misirlioglu et al. [3] | 3.05 |
| Moya et al. [6] | 2.801 |
| Oztop [7] | 2.980 |
| Badruddin et al. [12] | 3.2005 |
| Present simulation | 3.068 |

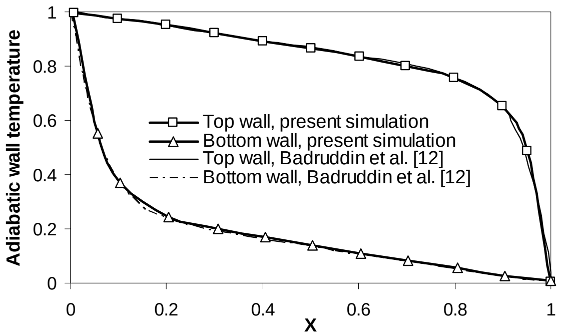


Figure 2. Simulation results in terms of adiabatic wall temperature compared with previously published works.

# 7. SIMULATION RESULTS

Simulation results in terms of dimensionless distributions of stream function, temperature, heat transfer irreversibility, and fluid friction irreversibility for the inclination angles of $\phi$=π/4, 3π/4, 5π/4, and 7π/4 are depicted in Figures 3-6 that correspond to $Ra=100$ and $R_d=4.0$.

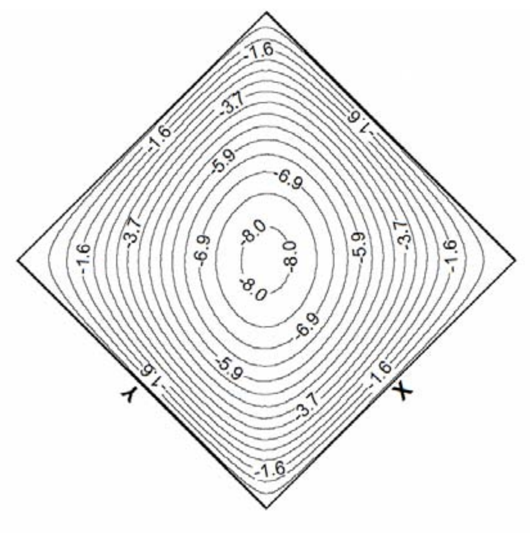


(a) Stream function, $\Psi$

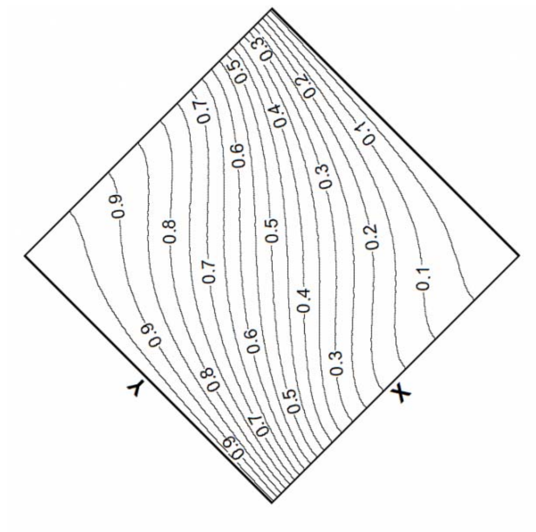


(b) Temperature, $\Theta$

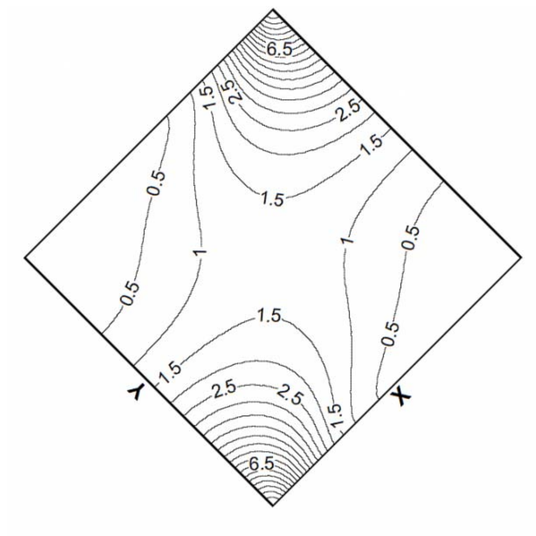


(c) Heat transfer irreversibility, $HTI$

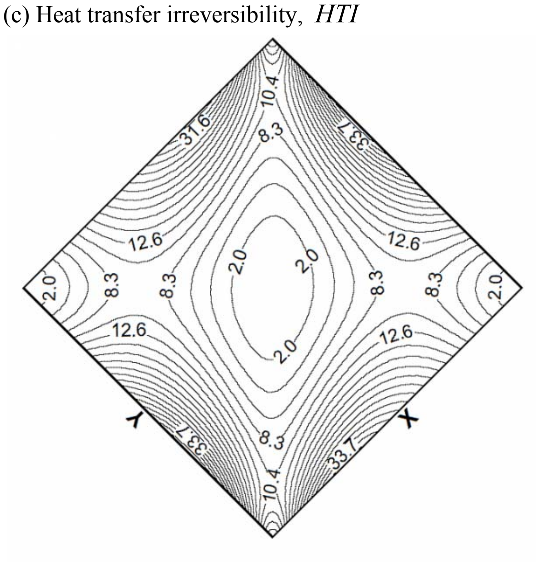


(d) Fluid friction irreversibility, $FFI$

Figure 3. Dimensionless distributions of flow, heat transfer, and entropy generation parameters inside the cavity with $\phi$=π/4, $Ra=100,$ and $R_d=4.0$.

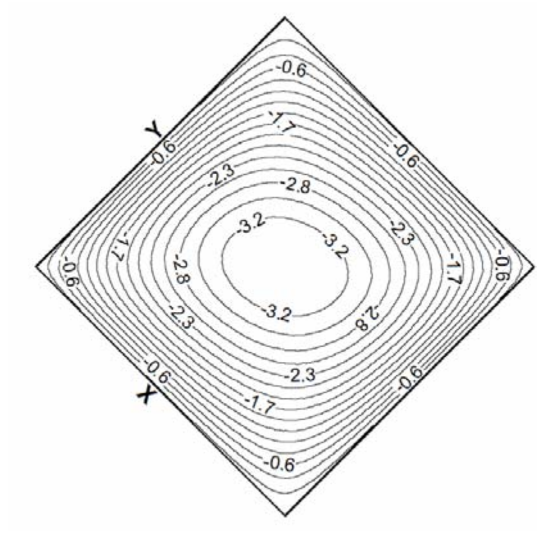


(a) Stream function, $\Psi$

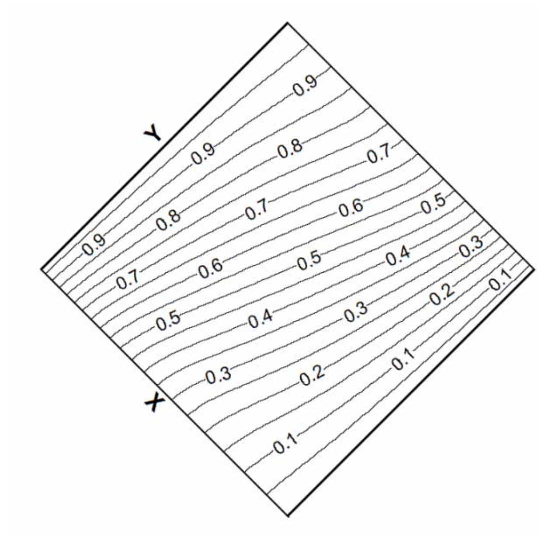


(b) Temperature, $\Theta$

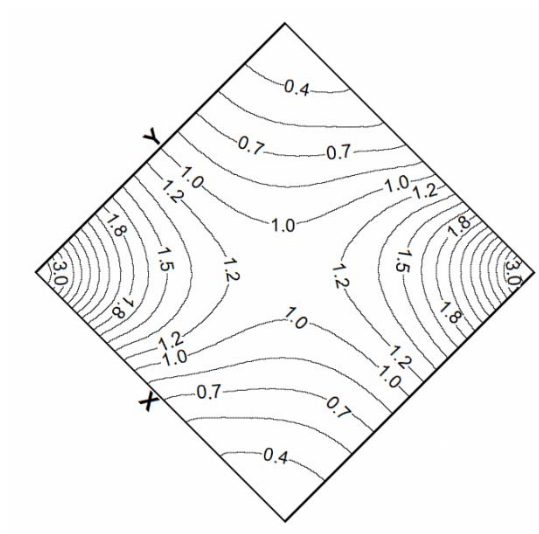


(c) Heat transfer irreversibility, *HTI*

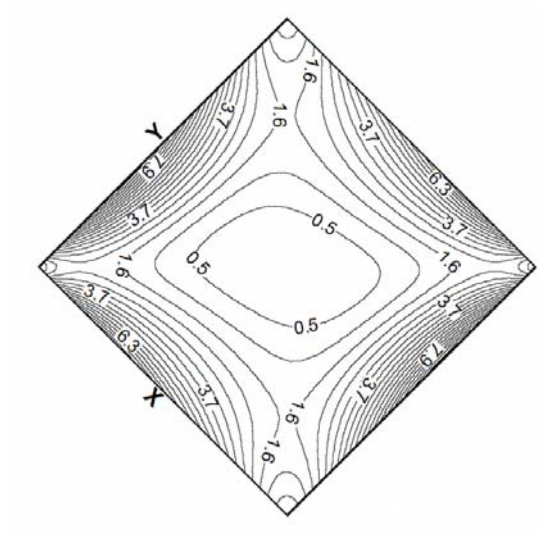


(d) Fluid friction irreversibility, *FFI*

Figure 4. Dimensionless distributions of flow, heat transfer, and entropy generation parameters inside the cavity with $\phi$=3π/4, *Ra=100,* and $R_d$*=4.0*.

Inspection of the streamlines as well as the isothermal lines demonstrates that, close to the hot wall (i.e., the wall indicated with y-axes), the fluid becomes heated and expands. This gives rise to an ascending motion. The fluid then changes its direction when reaching the neighborhood of the adiabatic wall. Thereafter, it releases heat at the cold wall, becomes denser, and sinks down. These happenings result in the establishment of a closed-loop for fluid flow which transfers heat from the hot wall to the cold wall that is clockwise in $\phi$=π/4, 3π/4 and contourclockwise in $\phi$ =5π/4, 7π/4. Notice that, while the direction of fluid rotation in $\phi$=π/4 and $\phi$=7π/4 are distinct, the corresponding streamlines and isothermal lines are comparable. This occurs due to geometric similarity of these two cases and can also be observed if one compares simulation results of the inclination angle of $\phi$=3π/4 with those of $\phi$=5π/4.

The presented results for fluid friction irreversibility and heat transfer irreversibility demonstrate that, in all of the aforesaid orientations, the values of *FFI* are higher than those of *HTI*. This implies that, irreversibility is dominated here by fluid friction effects. In a general way also notice that, mid parts of the walls act as strong concentrators of *FFI* since streamlines are concentrated there. Meanwhile, it is evident that, maximum values of *HTI* occur in those corners where fluid experiences a constant-temperature wall during its clockwise or counterclockwise rotation. Moreover, the figures show that both *HTI* and *FFI* of $\phi$=π/4, 7π/4 are much higher than those of $\phi$=3π/4, 5π/4. Concerning this, one may conclude that, the orientations with the hot wall in the bottom generate more entropy as compared with those with the hot wall in the top. This can be more quantitatively observed in Table 3 wherein global entropy generation rates for the aforesaid orientations are presented.

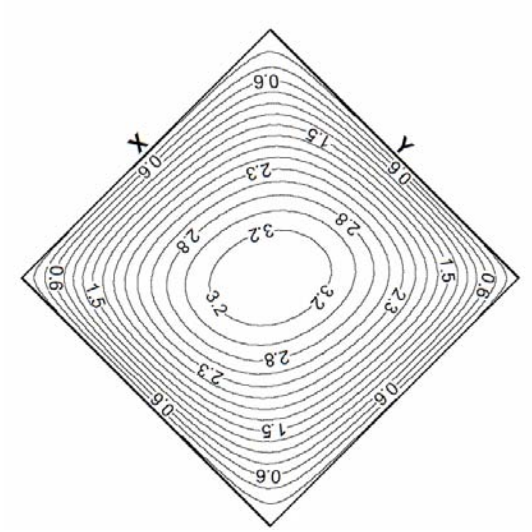


(a) Stream function, $\Psi$

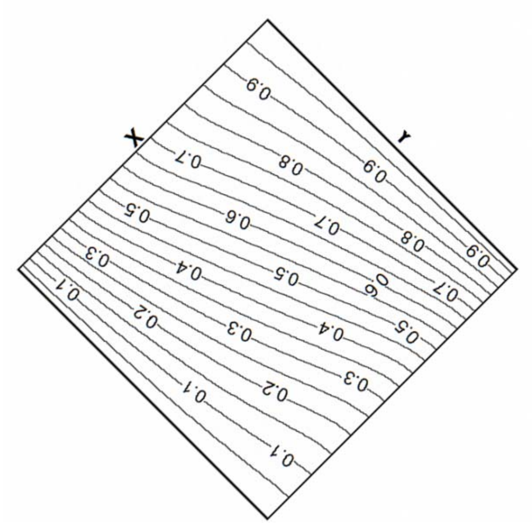


(b) Temperature, $\Theta$

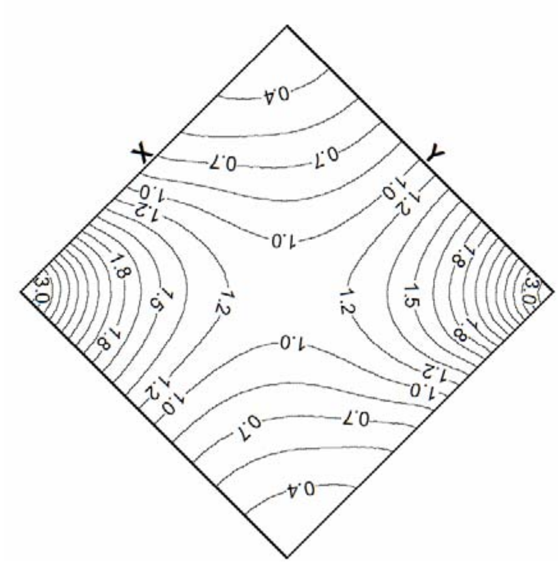


(c) Heat transfer irreversibility, $HTI$

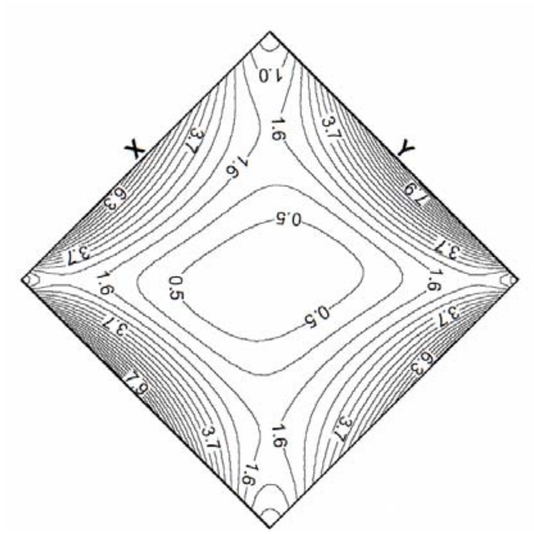


(d) Fluid friction irreversibility, $FFI$

Figure 5. Dimensionless distributions of flow, heat transfer, and entropy generation parameters inside the cavity with $\phi$=5π/4, $Ra=100$, and $R_d=4.0$.

Table 3. Effect of inclination angle on heat transfer and entropy generation parameters.

| Inclination angle ($\phi$) | $N_{global}$ | $\overline{Nu}$ | $\overline{Nu}/N_{global}$ |
|---|---|---|---|
| $\pi/4$ | 14.059 | 8.611 | 0.612 |
| $3\pi/4$ | 3.585 | 6.809 | 1.899 |

To demonstrate how orientation of the porous cavity may affect heat transfer characteristics therein, numerical values of average Nusselt number at the non-adiabatic walls for the current inclination angles are presented in Table 3. The influence of inclination angle on the average Nusselt number is obvious. Notice that, the orientations with the hot wall in the bottom lead to more heat transfer rates as compared with those with the hot wall in the top.

In summary, it has been demonstrated that, although cavities with $\phi$=π/4, 7π/4 suffer from the highest entropy generation rates, they achieve the best heat transfer characteristics. From the standpoints of the First Law and the Second Law of thermodynamics, an efficient orientation must lead to high heat transfer as well as low entropy generation. Consequently, the performance of the current orientations can be evaluated in terms of $\overline{Nu}/N_{global}$, which is the ratio of average Nusselt number to global entropy generation rate. Table 3 illustrates this quantity for different orientations. Concerning this table, it can be concluded that, the orientations with the hot wall in the top attain the highest values of $\overline{Nu}/N_{global}$ and achieve the optimum case with respect to heat transfer as well as entropy generation. Nevertheless, the orientations with the hot wall in the bottom are found inappropriate and must be avoided both from the First Law and the Second Law points of view.

Previous computations have been undertaken for *Ra=100*. To examine if Darcy-modified Rayleigh number of the problem at hand may alter the drawn conclusion for optimum orientation, computation are repeated here for *Ra=10* and *Ra=1000* and the corresponding results in terms of $\overline{Nu}/N_{global}$ are presented in Table 4. It is obvious that our conclusion can be easily generalized to a wide range of Darcy-modified Rayleigh number. Notice also that, with increase in $Ra$, the influence of cavity orientation becomes more and more pronounced. This implies that, with high values of Darcy-modified Rayleigh number, selection of appropriate orientation for the porous cavity is crucial both from the standpoints of the First Law and the Second Law of thermodynamics.

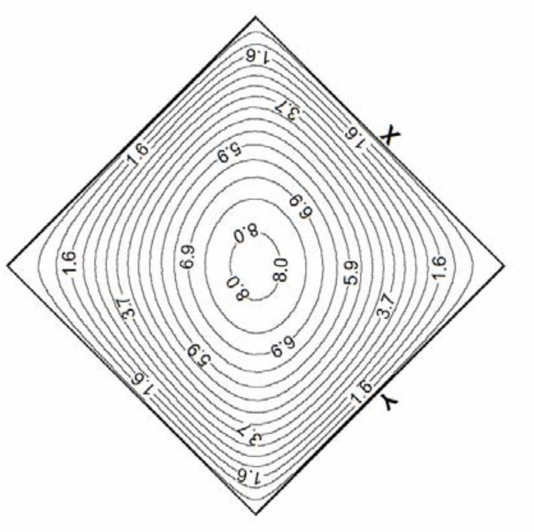


(a) Stream function, $\Psi$

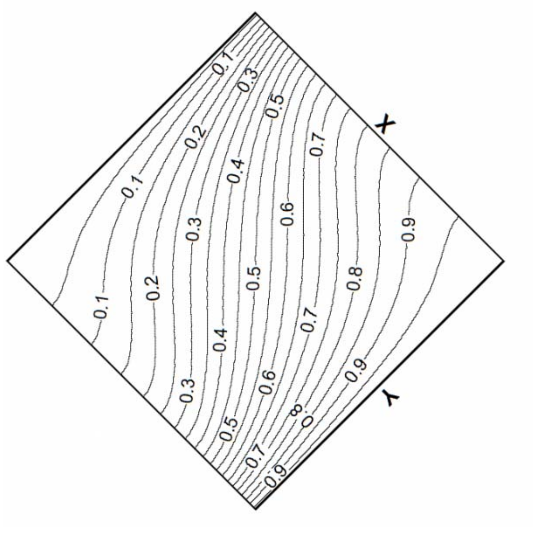


(b) Temperature, $\Theta$

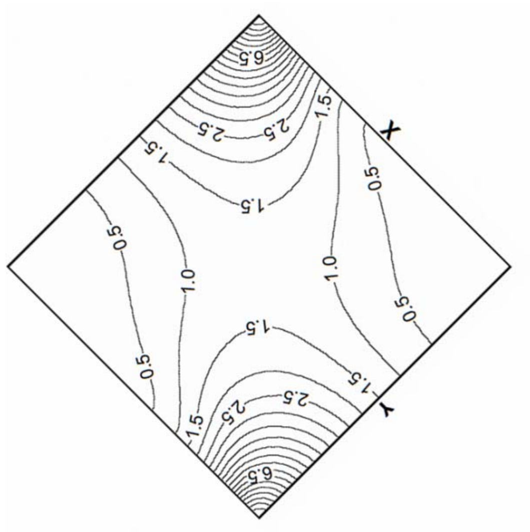


(c) Heat transfer irreversibility, $HTI$

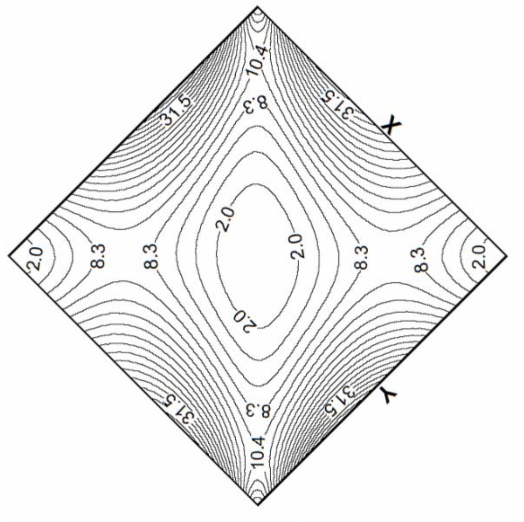


(d) Fluid friction irreversibility, $FFI$

Figure 6. Dimensionless distributions of flow, heat transfer, and entropy generation parameters inside the cavity with $\phi=7\pi/4$, *Ra=100,* and $R_d=4.0$.

Table 4. Ratio of average Nusselt number to global entropy generation rate for different Darcy-modified Rayleigh numbers.

| Inclination angle ($\phi$) | Ra = 10 | Ra = 100 | Ra = 1000 |
|---|---|---|---|
| $\pi/4$ | 6.068 | 0.612 | 0.035 |
| $3\pi/4$ | 6.126 | 1.899 | 0.243 |

## 8. CONCLUDING REMARKS

Buoyancy-driven flow inside an oblique cavity filled with a fluid-saturated porous medium was analyzed in this study. It was demonstrated that, in the current cases, irreversibility is dominated by fluid friction effects. Moreover, it was found that, orientations with the hot wall in the top achieve the optimum case from the standpoints of the First Law and the Second Law of thermodynamics.

## ACKNOLEDGMWNT

The author would like to thank the Islamic Azad University for financially supporting this research.

## NOMENCLATURE

| | |
|---|---|
| $a$ | mean absorption coefficient |
| $c_p$ | constant pressure specific heat (J/kg.K) |
| $Ec$ | Eckert number |
| $FFI$ | fluid friction irreversibility |
| $g$ | gravitational acceleration (m/s$^2$) |
| $HTI$ | heat transfer irreversibility |
| $k$ | thermal conductivity (W/m.K) |
| $K$ | permeability (m$^2$) |
| $L$ | cavity height (m) |
| $N$ | local dimensionless entropy generation rate |
| $N_{global}$ | global dimensionless entropy generation rate |
| $Nu_y$ | local Nusselt number |
| $\overline{Nu}$ | average Nusselt number |
| $p$ | pressure (Pa) |
| $q_r$ | radiative heat flux |
| $Ra$ | Darcy-modified Rayleigh number |
| $R_d$ | radiation parameter |
| $T$ | temperature at any point (K) |
| $T_C$ | temperature of the cold wall (K) |
| $T_H$ | temperature of the hot wall (K) |
| $\Delta T$ | temperature difference, $\Delta T = T_H - T_C$ (K) |
| $u, v$ | velocity components in x- and y-directions (m/s) |
| $x, y$ | Cartesian coordinates (m) |
| $X, Y$ | dimensionless coordinates |

*Greek symbols*

| | |
|---|---|
| $\alpha$ | effective thermal diffusivity (m$^2$/s) |
| $\beta$ | volumetric expansion coefficient (K$^{-1}$) |
| $\mu$ | dynamic viscosity (kg/m.s) |
| $\upsilon$ | kinematic viscosity (m$^2$/s) |
| $\rho$ | density (kg/m$^3$) |
| $\sigma$ | Stefan-Boltzman constant (W/m$^2$.K$^4$) |
| $\phi$ | inclination angle |
| $\psi$ | stream function (m$^2$/s) |
| $\Psi$ | dimensionless stream function |
| $\Theta$ | dimensionless temperature |
| $\tau$ | dimensionless temperature difference, $\Delta T / T_C$ |

## REFERENCES

1. Baytas A.C. and Pop I., 1999. Free convection in oblique enclosures filled with a porous medium, International Journal of Heat and Mass Transfer 42:1047–1057.
2. Saeid N.H. and Pop I., 2004. Transient free convection in a square cavity filled with a porous medium, International Journal of Heat and Mass Transfer 47:1917–1924.
3. Misirlioglu A., Baytas A.C., and Pop I., 2005. Free convection in a wavy cavity filled with a porous medium, International Journal of Heat and Mass Transfer 48:1840-1850.
4. Zahmatkesh I., 2008. On the importance of thermal boundary conditions in heat transfer and entropy generation for natural convection inside a porous enclosure, International Journal of Thermal Sciences 47:339–346.
5. Zahmatkesh I., 2012. Second-law analysis of buoyancy-driven flow inside a rectangular porous enclosure with three adiabatic walls, Majlesi Journal of Energy Management 1:343–352.
6. Moya S.L., Ramos E., and Sen M., 1987. Numerical study of natural convection in a tilted rectangular porous material, International Journal of Heat and Mass Transfer 30:741–756.
7. Oztop H.F., 2007. Natural convection in partially cooled and inclined porous rectangular enclosures, International Journal of Thermal Sciences 46:149–156.
8. Dawwod A.S. and Ismaeel M.E., 2008. Numerical study of natural convective heat transfer in an inclined square porous layer, Al-Rafidain Engineering Journal 16:81–95.
9. Baytas A.C., 2000. Entropy generation for natural convection in an inclined porous cavity, International Journal of Heat and Mass Transfer 43:2089–2099.
10. Heidary H., Pirmohammadi M., and Davoudi M., 2012. Control of free convection and entropy generation in inclined porous media, Heat Transfer Engineering 33:565-573.
11. Zahmatkesh I., 2007. Influence of thermal radiation on free convection inside a porous enclosure, Emirates Journal for Engineering Research 12:47-52.
12. Badruddin I.A., Zainal Z.A, Narayana P.A.A., and Seetharamu K.N., 2006. Heat transfer in

porous cavity under the influence of radiation and viscous dissipation, International Communications in Heat and Mass Transfer 33:491–499.

13. Sigel R. and Howell J.R., 1992. Thermal Radiation Heat transfer, Hemisphere, New York.
14. Patankar S.V., 1980. Numerical Heat Transfer and Fluid Flow, Hemisphere/McGrawHill, Washington DC.